DOI 10.24425/aee.2024.149922

Design of a novel control scheme for the operation of the doubly fed induction generator

RAM KRISHAN KUMAR✉, **JAYANTI CHOUDHARY**

Electrical Engineering Department, National Institute of Technology Patna (800005) Bihar, India

e-mail: {✉ ramk.pg18.ee/Jayanti}@nitp.ac.in

(Received: 14.06.2023, revised: 18.04.2024)

Abstract: The advancement of ocean renewable energy through Tidal Stream Turbines (TSTs) necessitates the use of a variety of computer models to properly evaluate TST efficiency. The Doubly Fed Induction Generator (DFIG) is the most widely utilized Wind Turbine (WT) in the expanding global wind sector. Grid-tied wind energy systems often use the DFIG to meet conventional grid needs including power quality enhancement, grid stability, grid synchronization, power regulation, and fault ride-through. This paper demonstrates the design of a novel control scheme for the operation of the DFIG. The suggested control scheme consisted of an Improved Recurrent Fuzzy Neural Network (IRFNN) and Ant Colony Optimization with Genetic Algorithms (GACOs). A global control system is created and executed to monitor the changeover between the two operating modes. The plant enters a variable speed mode when the tidal speed is low enough, where the system is controlled to ensure that the turbo-generator module functions at peak power extraction efficiency for any specific tidal velocity. The findings demonstrate the system's superior efficiency, with the highest power extraction provided despite variations in tidal stream input.

Key words: DFIG, GACO, improved recurrent fuzzy neural network (IRFNN), modelling, TST

1. Introduction

Energy from abundant and transparent sources like the sun and the wind, known as Renewable Energy Resources (RESs) and Distributed Generations (DGs), have garnered a lot of interest as a potential solution to the world's growing energy need. Among the many RESs, wind power is gaining popularity for a variety of reasons, including environmental and economic ones. In today's

power grids, wind farms account for a significant share of the overall energy production. Efficient management of renewable energy sources is challenging due to variability in power output from wind farms [1, 2].

A novel induction machine, the brushless doubly fed induction generator (BDFIG) has two independent stator windings and a specialized rotor. The BDFIG, which eliminates the need for brushes and slide rings, increases the dependability of wind turbine systems while decreasing the cost of maintenance for such systems as offshore wind power plants. The low voltage ride through (LVRT) ability is enhanced, and the mechanical gearbox is smaller [1].

The usage of renewable energy sources including thermal energy, tidal energy, and marine tidal energy gives the benefit of sustainability in all areas of the energy sector growth in current decades. There has been rapid growth in innovative marine tidal energy systems. The enormous possibility for tidal energy in Europe is the driving force behind these endeavors. 42% of Europe's tidal energy is in France, 48% in the United Kingdom, and 8% in Ireland [1–3]. As tidal turbines must operate underwater, they are susceptible to a variety of problems, including grid faults, driven through the marine environment and the elements. The weather is a major contributor to grid problems (37% in Iceland, 23% in Denmark, and 21% in Norway) [4].

Vector Oriented Control (VOC) and Direct Power Control (DPC) are the most often employed regulator techniques for the DFIG. A Phase-Locked Loop (PLL) is needed because the VOC decouples three-phase components in the setting of a rotating reference frame for which the VOC requires [5, 6]. The linear control methodology framework can be employed for the examination of the Linear Time-Invariant (LTI) characteristics of the control structure [7]. DFIGs controlled by VOC rely on PLL for performance and parameter adjustment. DPC offers an alternative by allowing DFIGs to directly regulate power output without the need for PLL and complex parameter adjustments, simplifying the control method. [8, 9]. The typical DPC selects switching signals using a Look-Up Table (LUT) structure [10]. In LUT-based DPC, the switching frequency isn't fixed and varies over time, causing power and torque fluctuations in many applications [11]. Model Predictive Control (MPC)-DPC is a newly implemented DPC approach in DFI [12, 13]. The controlled impact of MPC-DPC is ensured by the collection of the voltage vector in the most optimum manner. A large amount of time was required for the assessment of the optimum control vector, increasing the computational burden imposed on the control system.

In combination with DPC, the Back-Stepping (BS) algorithm is being developed [14]. A system that is easy to understand and performs well in steady-state. However, since BS-DPC is based entirely on the Proportional Integral (PI), it is difficult to achieve zero steady-state error in the presence of shocks or model mismatches. There is a proposal for a coordinated (C)-DPC without PLL [15]. A virtual phase signal is substituted for the PLL as the coordinate transformation signal. Performance was formerly vulnerable to variations in grid frequency, but it now exhibits exceptional steady-state performance. When using a Back-to-Back (BTB) converter in combination with Voltage Modulated DPC (VM-DPC), it has the following features:

- DPC and LTI systems: The suggested VM-DPC is used to convert the DFIG scheme to an LTI one. It could be studied and developed using several linear control approaches.
- Simple and easy implementation: The control method that has been suggested makes use of a feed-back structure design and simple feed-forward. Additionally, the Rotor Side Converter (RSC) and Grid Side Converter (GSC) do not use the PLL, or Park transforms, so the structure and calculation may be reduced in comparison to the VOC.

– Guaranteed exponential stability: With the use of eigenvalue analysis, it has been shown that the suggested VM-DPC can steady the DFIG in the weak-grid combination situation, which is difficult to do with current DPC methods.
– Improved performance: A quicker transient reaction is achieved by the suggested VM-DPC in comparison to traditional VOC. Furthermore, it retains a good steady-state efficiency on an equal footing with the VOC. In addition, the method's resilience against variable mismatches and distorted grid conditions is shown [16].

1.1. Model of doubly fed induction generation (DFIG)

DFIG vector control must be established to operate rotor flux components such as [17]:

$$\begin{cases} \Psi_{dr} = L_r I_{dr} + M I_{dr} \\ \Psi_{qr} = L_r I_{qr} + M I_{qr} \end{cases}, \tag{1}$$

where: L_r is the rotor inductance, Ψ_{qr} and Ψ_{dr} are two components of rotor fluxes, M denotes the mutual inductance, while I_{qr} and I_{dr} denote the rotor currents, respectively.

Components of the stator flux

$$\begin{cases} \Psi_{ds} = L_s I_{ds} + M I_{ds} \\ \Psi_{qs} = L_s I_{qs} + M I_{qs} \end{cases}. \tag{2}$$

For example, the stator fluxes are Ψ_{qs} and Ψ_{ds}, while the stator inductance is L_s in the following equation:

The voltage components of the stator are

$$\begin{cases} V_{dr} = I_{dr} R_r - \omega_r \Psi_{qr} + \dfrac{\mathrm{d}}{\mathrm{d}t} \Psi_{dr} \\ V_{qr} = I_{qr} R_r + \omega_r \Psi_{dr} + \dfrac{\mathrm{d}}{\mathrm{d}t} \Psi_{qr} \end{cases}, \tag{3}$$

where: R_r is the rotor resistance, V_{dr} and V_{qr} are the rotor voltages.

The reactive powers and stator active are defined as

$$\begin{cases} P_s = 1.5(V_{ds} I_{ds} + V_{qs} I_{qs}) \\ Q_s = 1.5(V_{qs} I_{ds} + V_{ds} I_{qs}) \end{cases}. \tag{4}$$

Q_s denotes the reactivity of the system, whereas P_s denotes the activity.

Mathematically, the electromagnetic torque is stated as follows:

$$T_e = \frac{3}{2} p \frac{M}{L_r} \left(I_{dr} \Psi_{qs} - I_{qr} \Psi_{ds} \right). \tag{5}$$

T_e is the electromagnetic torque, and p is the quantity of poles.

The following mechanical equation completes the electric model of the DFIG.

$$T_e - T_r = J \frac{\mathrm{d}\Omega}{\mathrm{d}t} + f_r \Omega, \tag{6}$$

where: f is the viscosity-coefficient of viscosity, Ω is the mechanical rotor speed, J is the inertia, T_r is defines as the load torque.

1.2. Smart grid-integrated wind energy reliability challenges confined to IEC 61400-25-26/1/2/3 standards

International Electrotechnical Commission (IEC) standards, in particular IEC 61400-25-26/1/2/3, address the many reliability concerns introduced by the smart grid's use of wind energy. The emphasis of these guidelines is on the information and data interchange between wind turbines and the electricity grid, which is crucial to the system's reliability and efficiency. Maintaining reliable connections and interoperability across smart grid components is a major obstacle. Wind generators, grid operators, and control systems all fall under this category. Information may be shared using a standardized protocol and data model according to the IEC 61400-25-26/1/2/3 standards. These standards offer a framework to assure compatibility and interoperability across devices and systems, allowing for easy and effective communication and operation [2].

Managing the grid's stability and electricity quality as wind energy output fluctuates is another difficulty. The unpredictability of wind makes wind power production fundamentally intermittent. Grid stability and electricity quality may be affected by this variation. Wind turbine control systems that provide grid support services must adhere to regulations defined by the IEC. Active power control and reactive power regulation are two of these roles, and they both contribute to grid stability and adequate power quality. Large-scale wind farm grid interconnection also has its own unique issues. Integration challenges increase when wind farms grow in size and spread out over a wider area. These issues are addressed by the guidelines and regulations for wind farm grid interconnection provided by the IEC 61400-25-26/1/2/3 standards. These guidelines guarantee that wind farms are coordinated and controlled effectively so that they do not degrade the grid's efficiency or dependability.

In sum, the IEC 61400-25-26/1/2/3 standards are vital in resolving the dependability issues that arise from adding wind power to the smart grid. These standards assist assure the stable and effective functioning of the smart grid system by creating communication protocols, grid support functions, and rules for wind farm integration, all of which encourage the wider use of wind energy as a clean and sustainable power source. The following study expands on the design of a novel control system for the operation of DFIG. Several researchers explained their findings as seen below.

Wang Y. *et al*. (2023) [18] suggested a new sensor-less speed estimate approach that makes use of the easily accessible data from the generator drive controller to measure the speed of the DFIG used in WTs. Next, to provide a faster real-time estimate rate, and offer a parabolic overlapping window interpolation technique to follow the spectral content as a function of controller signal speed. According to the findings of the experiments, it is possible to achieve a high estimate rate with high accuracy in the distinctive transient dynamics of field applications.

Tavoosi J. *et al*. (2022) [19] provide a novel fuzzy approach to controlling the active and reactive power of a power grid that incorporates renewable energy sources like WTs and DFIGs. The DFIG-equipped WT's RSC is controlled by a Recurrent Type-II Fuzzy Neural Network (RT2FNN) controller built on Radial Basis Function Networks (RBFNs). The MATLAB findings demonstrate the superior efficiency, robustness, excellent correctness, and power superiority enhancement of the designed regulator in wind driven DFIGs.

Sahri Y. *et al*. (2021) [20] created the anticipated system dynamics to emphasize the effectiveness of the suggested scheme, a unique control technique was developed. A Twelve-Sector Direct Torque Controller (12-DTC) is included in the suggested controller. The simulated findings

showed that the suggested strategy outperformed the others by a wide margin with less rotor flux and electromagnetic torque ripples and higher produced influence excellence and lower Total Harmonic Distortion (THD) currents C-DTC and 12-DTC.

Alhato M. *et al*. (2020) [21] present a new approach to designing PI regulators for a DFIG in wind energy that makes use of Thermal Exchange Optimization (TEO) to achieve maximum efficiency. In addition, a statistical analysis using Friedman and Bonferroni-tests Dunn's reveals that in contrast to the other described metaheuristic approaches, the TEO approach generates much more relevant data.

Moreira A. *et al*. (2019) [22] describe and validate a new control method for power production and electric grid harmonic adjustment by comparing it to existing solutions. The new technique is used to analyse the harmonic filtering behavior of operation points. Simulation and experimental findings are used to validate the suggested system's efficacy. The THD of the grid current without using any of the provided solutions is 17.21%. When approach 1 is used, the THD drops to 5.68%. When method 2 is used, the THD is reduced to 3.18%.

Abdelmalek S. *et al*. (2018) [23] provide a novel Fault-Tolerant Tracking Control (FTC) approach for a DFIG-based WT in the presence of actuator defects using a combination of fuzzy observers. The primary innovation is a new FTC that uses an insignificant controller logic. The goal of the controller is to keep track of the system's reference states reliably despite the failures in the actuators and to estimate the system's state and failures simultaneously. A mathematical model is performed on a characteristic 1.5-megawatt DFIG-based WT scheme to assess the performance of the suggested control method compared to the current findings.

Venkatesh M. *et al*. (2017) [24] employ a PI controller to control the DFIG's active and reactive power; then use the Particle Swarm Optimization (PSO) method to fine-tune the PI controller. The findings achieved by using the suggested approach demonstrate that it is efficient in enhancing the transient reaction of active power and reactive power of the DFIG, resulting in reduced oscillations in the powers of the DFIG. As a result, DFIG's terminal voltage becomes constant. The suggested technique also guarantees the decoupling of DFIG's active and reactive power supplies.

Boudjema Z. *et al*. (2017) [25] introduced an improved DTC scheme for a Wind Energy Conversion System's (WECS) DFIG via the use of space vector modulation and second-order continuous sliding mode. The suggested DTC approach decreases flux, current, and torque ripples by using second-order continuous sliding mode control. Sliding surfaces are used to direct the deviation from the reference value to areas where the deviation must be zero. The suggested DTC approach is shown to be more successful than the C-DTC strategy in simulations.

Ghefiri *et al*. (2017) [26] proposed a novel complimentary control technique to maximize the power output of a TST consisting of a hydrodynamic turbine, a DFIG, and a back-to-back power converter. The RSC utilizes a rotational speed controller based on maximum power point tracking (MPPT) to enhance output power. The collected findings demonstrate that the proposed controls improve the performance of the output power in various operating modes. For $V = 3$ m/s, the generated torque peaks at 1.03×105 Nm, while for $V = 2$ m/s, it reaches a low of 4.58×104 Nm.

Ebrahimkhani S. *et al*. (2016) [27] provide a new strong Fractional-Order Sliding Mode (FOSM) controller for MPPT management of a DFIF-based WECS. The estimation of uncertainties and disturbances is performed via a fractional order ambiguity estimator to improve the control system's reliability. Lyapunov's theory of stability is used to demonstrate the closed-loop signals'

boundedness and convergent features. The efficiency and robustness of the suggested control strategy were established using simulated results obtained under a wide range of uncertainty conditions.

There is a wide range of authors who used the technique and presented their discoveries, as given in Table 1.

Table 1. Summarize the table of reviewed literature

Authors	Techniques	Outcomes
Wang Y. *et al.* (2023) [18]	Parabolic Interpolation	The findings show that accurate speed estimate in real-time is possible over the whole working range of the DFIG, from sub-synchronous to super-synchronous speeds, and under a wide variety of loads.
Tavoosi J. *et al.* (2022) [19]	RT2FNN	The experimental findings show that the presented RT2FNN controller outperforms T2FNN and traditional PI controllers in terms of efficiency, reaction time, and the number of mistakes made in both transient and steady states.
Sahri Y. *et al.* (2021) [20]	DTC	The simulated findings demonstrated significantly adequate efficiency, with a significant decrease in ripples in torque and flux, strong dynamic responses, and a low THD (1.8%) of the produced current at a continuous grid frequency of 50 Hz.
Alhato M. *et al.* (2020) [21]	TEO	The findings show that the suggested TEO-based technique is a beneficial way to regulate WECS by modifying the gains of the unidentified PI controllers.
Moreira A. *et al.* (2019) [22]	RSC and GSC	The measured THD of grid current has dropped from 17.34% (instance 1) to 5.68% (instance 2) and 3.18% (instance 3), as shown by the experiment results.
Abdelmalek S. *et al.* (2018) [23]	FTC	The suggested FTC with a nominal controller is demonstrated to effectively integrate failures, compensate for the consequences of actuator faults, and accomplish the solidity convergence of the global closed-loop system in both nominal and faulty functioning in the simulated findings.
Venkatesh M. *et al.* (2017) [24]	PSO	The findings produced by using the suggested approach demonstrate that it is successful in enhancing the transient responsiveness, resulting in reduced oscillations in the powers of the DFIG.
Boudjema Z. *et al.* (2017) [25]	DTC	Based on these findings, a robust control approach like SOCSM-DTC might be a highly appealing option for devices employing the DFIG like WECSs.
Ghefiri *et al.* (2017) [26]	MPPT	The collected findings demonstrate that the proposed controls improve the performance of the output power in various operating modes.
Ebrahimkhani S. *et al.* (2016) [27]	FTC	The modelling findings show that the suggested controller is efficient and resilient to parameter fluctuations and disturbances. It is possible to reliably compute difficulties with high frequency and large amplitude components if the fractional order estimating variables are configured properly.

Many recent academic works have presented cutting-edge control and optimization strategies for wind energy conversion systems that use DFIGs. Fuzzy control, DTC, and optimization techniques like PSO and TEO are among examples. Their end goal is to increase the DFIGs' power production, efficiency, and dependability in wind turbines. The spinning blades of TSTs, which are built to harness the kinetic energy of moving water, pose threats to marine life, and can even hasten the extinction of some species. The noise these turbines produce has raised concerns about their possible impact on fish populations. Moreover, TSTs can alter sedimentation and water quality. One difficulty is that TSTs produce very little power at low tidal speeds but considerably more at high speeds. To solve these problems, this study proposes a novel approach, including Improved Recurrent Fuzzy Neural Networks (IRFNNs) and Genetic Algorithm-based Controller Optimization (GACO), with encouraging results.

2. Research objectives

– To create architecture for a controller used to manage the speed and reactive power of a DFIG.
– Using the hyperstability idea and the ACO mechanism, to evaluate and implement a way to confirm the stability of the proposed estimating approach.
– Using the DFIG that act as an externally regulated variable-speed induction generator with a regulated rotor circuit. AC–DC–AC power converters connect the generator's stator to the public power grid.

3. Research methodology

This section describes the working infrastructure of the DFIG model GOCA and IRFNN controller related to the proposed methodology as shown in Fig. 1. The configuration of a DFIG-based TST system. The DFIG is an induction generator with a rotor circuit that could be controlled using the DFIG controller to allow for operation at different speeds. Using AC–DC–AC power converters, the generator's stator is linked to the grid.

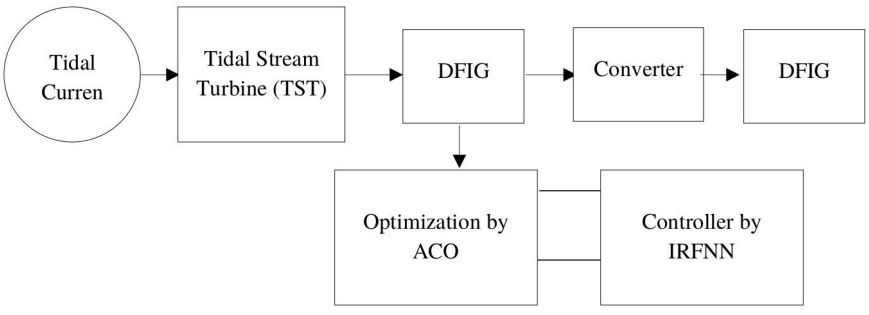

Fig. 1. Proposed methodology

The tidal turbine's output is regulated by factors like these:

$$P_t = \frac{1}{2} C_p(\lambda, \beta) \rho \pi R^2 V^3, \tag{7}$$

where P_t is the power generated by the turbines (W). The diameter of the turbine blades is measured in meters, and the power coefficient is denoted by C_p. It is possible to find the expression of C_p by using an approximation function that is dependent on the blades pitch angle $\beta(\circ)$ and the tip-speed ratio λ, which is distinct as below:

$$\lambda = \frac{\omega_t R}{V}, \tag{8}$$

where the rotor's speed, expressed in rad/s, is given by the expression ω_t.

Figure 1 shows how much hydrodynamic torque is generated by the tidal turbine in terms of (Nm).

$$T_{\text{tst}} = \frac{P_t}{\omega_t}. \tag{9}$$

– **DFIG model**

The DFIG-based TST would have several benefits, including the capacity to create power at variable speeds depending on the active and reactive power capacities of four quadrants in each quadrant. The DFIG, on the other hand, is a long-lasting and low-maintenance product. The dynamic classical of the generator is developed in the synchronous d–q frame utilizing Park's conversion for the control strategy, as explained in detail. The following are the (V) expressions for the d–q axis voltages of the stator and rotor [28].

$$\begin{cases} U_{sd} = R_s I_{sd} + \dfrac{\mathrm{d}\varphi_{sd}}{\mathrm{d}t} - \omega_s \varphi_{sq} \\ U_{sq} = R_s I_{sq} + \dfrac{\mathrm{d}\varphi_{sq}}{\mathrm{d}t} - \omega_s \varphi_{sd} \\ U_{rd} = R_r I_{rd} + \dfrac{\mathrm{d}\varphi_{rd}}{\mathrm{d}t} - \omega_r \varphi_{rq} \\ U_{rq} = R_r I_{rq} + \dfrac{\mathrm{d}\varphi_{sq}}{\mathrm{d}t} - \omega_r \varphi_{rd} \end{cases}. \tag{10}$$

The rotor and stator flux direct quadrature components in (Wb) are well-defined as

$$\begin{cases} \varphi_{sd} = L_s I_{sd} + L_m I_{rd} \\ \varphi_{sq} = L_s I_{sq} + L_m I_{rq} \\ \varphi_{rd} = L_r I_{rd} + L_m I_{sd} \\ \varphi_{rq} = L_r I_{rq} + L_m I_{sq} \end{cases}. \tag{11}$$

D-q frames are used to represent DFIG electromagnetic torque.

$$T_{em} = \frac{3}{2} p L_m \left(I_{sq} I_{rd} - I_{sd} I_{rq} \right), \tag{12}$$

where currents flow along the I_{sdq}, I_{rdq} axis of both the stator and rotating disk (A), radians per second (rad/s) is represented by ω_s, ω_r, respectively, for the sake of clarity, we'll refer to these resistances (Ω) as R_s and R_r. There are three inductances (H): the rotor and stator inductances (L_s and L_r), the magnetizing inductance (L_m), and the pole pair number (p).

– **Convertors for back-to-back use**
Vector control may be achieved on both the generator and GSC by connecting two six-switch-based converters BTB and using an intermediary DC-link capacitor. The GOCA and the IRFNN controller are employed in the entire AC–DC–AC power converter that is being used. The vector control process is used to optimize the generator's operations according to the DFIG's dynamical model, which is distinct in the d–q frame by the ACO algorithm. The IRFNN's goal is to maintain a constant voltage autonomous of the rotor's magnitude and route of rotation. The reactive power is controlled using a vector control method.
It is possible to compute the system's (W/var) exchanged active and reactive power (W/var)

$$P_g = \frac{3}{2}\left(U_{dg}I_{dg} - U_{qg}I_{qg}\right), \tag{13}$$

$$Q_g = \frac{3}{2}\left(U_{qg}I_{dg} - U_{dg}I_{qg}\right), \tag{14}$$

where grid voltage and flows in the d and q situation frames may be referred to as U_{dg}, U_{qg} (V and A), respectively.
When the synchronized frame's d-axis and the grid voltage vector are parallel $\left(U_{dg} = U_g\right)$ and the grid voltage vector is perpendicular to the synchronized frame's q-axis $\left(U_{qg} = 0\right)$ VOC is generated.
Because of this, the following are the definitions of active and reactive power.

$$P_g = \frac{3}{2}U_g I_{dg}, \tag{15}$$

$$Q_g = \frac{3}{2}U_g I_{qg}. \tag{16}$$

To illustrate the connection between DC-link storage and grid power flow, it could use the following equation:

$$P_g = \frac{3}{2}U_g I_{dg} = U_{dc}i_{dc}. \tag{17}$$

$P_g = \frac{3}{2}U_g I_{dg}$: This part of the equation represents the electrical power (P_g) generated or controlled by the power controller. It's calculated as the product of the voltage (U_g) and the current (I_{dg}) in the system. The factor is included, likely as a scaling factor based on the system's characteristics.
$U_{dc}i_{dc}$: This part of the equation is another way to represent the electrical power (P_g). Here, represents the voltage (U_g) in the direct current (DC) circuit of the power controller, and represents the current (I_{dg}) in the same circuit. Multiplying these two values also gives you the electrical power (P_g) generated or controlled. So, both sides of the equation indeed represent the same electrical power, but they are expressed in different terms based on the components and characteristics of the power controller system.

– **Ant colony optimisation (ACO)**
ACO was first presented by Dorigo in 1992 [29]. The findings from studies on ant colonies as a social unit served as inspiration for this population-based heuristic evolutionary method. The ACO method has been shown to provide superior optimization results when used for issue-solving. Many people's efforts and data feedback are essential to the ACO method.

Although individual ant behavior is somewhat simplistic, the behavior of a colony is often seen as being rather commendable. The ACO method demonstrates features of decentralized programming, iterative improvement, and heuristic analysis. The evolutionary process is essentially a heuristic global optimization technique [30–34]. The pheromone-based exchange of information has been crucial to the evolutionary process. Several combinatorial optimization problems can be solved by using the ACO approach, such as the traveling salesman problem, assigning difficulty, task allocation difficulty, vehicle networking difficulty, graph colouring difficulty, and route optimization difficulty [36–38]. Figure 2 depicts the general architecture of ACO.

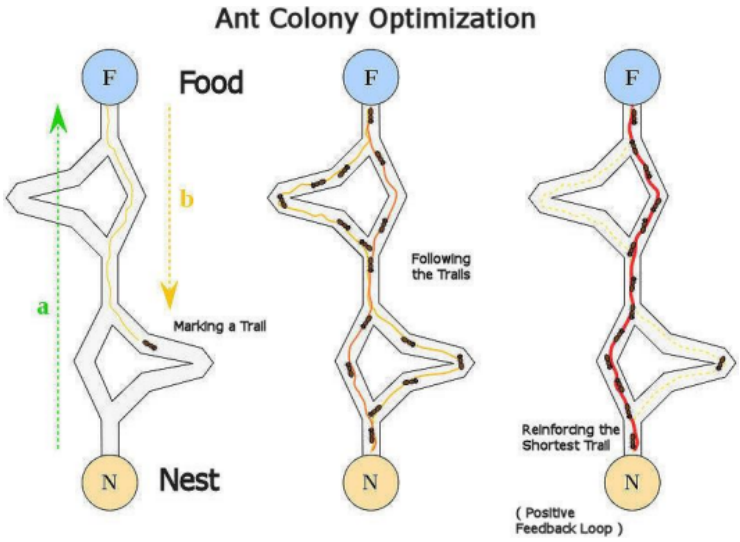

Fig. 2. Architecture of ACO [39]

ACO algorithm specialists have developed better ACO algorithms to handle complicated optimization issues. In recent years, some improved outcomes and impacts have been produced. Nevertheless, the difficulty of large-scale optimization issues is growing, and even the most recent and best ACO methods have constraints when it comes to addressing these types of issues, such as sluggish convergence rapidity, a local optimal value, etc. [40–46].

– **IRFNN controller**

Figure 3 depicts the dynamic feedback that helps students learn more quickly. Layer 2 and layer 3 comprise the memory terms, and $S_R = \sum_{R=1}^{m} O_R^{(3)}(k)\chi_{RR}$, The sigmoid function, which is analogous to a memory element, is a recurrent unit. Instead of using the MIN operation, they used the identical or fuzzy AND combination operations as a simple algebraic creation. Hence, it was shown that the suggested IRFNN could handle nonlinear issues, enhance convergence accuracy, and shorten training time. The following is a list of the node output for each tier.

$$O_i^{(1)}(k) = X_i^{(1)}(k), \quad i = 1, 2, \tag{18}$$

$$O_i^{(1)}(k) = \exp\left\{-\frac{\left(O_i^{(1)}(k) + O_{ij}^{(2)}(k-1).\phi_{ij} - m_{ij}\right)^2}{(\sigma_{ij})^2}\right\}, \tag{19}$$

$$f_R(k) = \frac{1}{1+\exp(-S_R)}, \tag{20}$$

$$O_R^3(k) = f_R \prod_{i=1}^{2} O_{ij}^2(k) w_{ij}, \tag{21}$$

$$O_E^3(k) = \sum_R O_R^3(k)\, w_{RE} = i_{qs}^*. \tag{22}$$

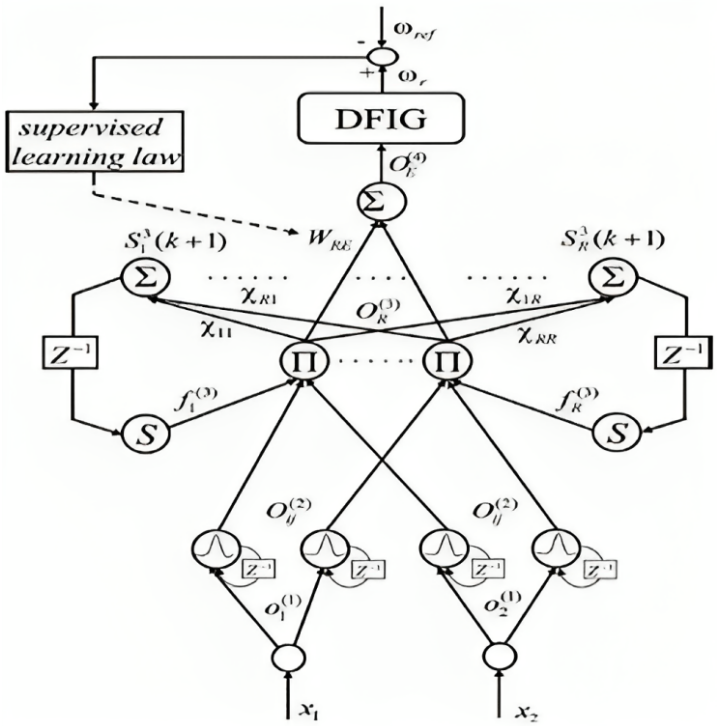

Fig. 3. Configuration of IRFNN

Expressed in terms of $e_(k)$ and $X_i^{(1)}(k)$ the input error of the reference speed to real speed, which is expressed as the difference between $\Delta e(k) = e(k) - e(k-1)\, e(k)$), the IRFNN iteration number k indicates this. The i-term input linguistic variable $O_i^{(1)}$ in the j-term has a mean and a standard deviation (STD) of m_{ij} and σ_{ij}. and σ_{ij}, $R \in \{1, 2, 3 \ldots, j \times j\}$, $w_{ij} = 1$, and χ_{RR} is the recurrent weight. Training the IRFNN requires the input values of σ_{ij}, m_{ij}, w_{RE}, ϕ_{ij}, and $O_E^{(4)}$ the output values of χ_{RR} the amount of work put in by the control system [47].

3.1. Proposed algorithm

1. **Power generated by turbines:**
   - Define the variables:
     - P_t: Power generated by the turbines (W),
     - C_p (λ, β): Power coefficient, a function of tip-speed ratio (λ) and pitch angle (β) of the turbine blades,
     - ρ: Air density (kg/m^3),
     - R: Diameter of the turbine blades (m),
     - V: Wind velocity (m/s).
   - Calculate P_t using Eq. (7): $P_t = 1/2 * C_p(\lambda, \beta) * \rho * \pi * R\text{^}2 * V\text{^}3$.
2. **Tip-speed ratio (λ) calculation:**
   - Define the variables:
     - ω_t: Rotor speed (rad/s).
   - Calculate λ using Eq. (8): $\lambda = (\omega_t * R)/V$.
3. **Hydrodynamic torque (T_{tst}) generated by the turbine:**
   - Calculate T_{tst} using Eq. (9): $T_{\text{tst}} = P_t/\omega_t$.
4. **DFIG model:**
   - Define the variables:
     - I_{sd}, I_{sq}: Stator current in the d–q axis (A),
     - φ_{sd}, φ_{sq}: Stator flux in the d–q axis (Wb),
     - I_{rd}, I_{rq}: Rotor current in the d–q axis (A),
     - φ_{rd}, φ_{rq}: Rotor flux in the d–q axis (Wb),
     - L_s, L_r, L_m: Stator, rotor, and magnetizing inductances (H),
     - R_s, R_r: Stator and rotor resistances (Ω),
     - p: Number of pole pairs.
   - Calculate stator and rotor voltages in the d–q axis using Eq. (10).
   - Calculate stator and rotor flux components in the d–q axis using Equation (11).
   - Calculate electromagnetic torque (T_{em}) using Eq. (12):
     $T_{em} = (3/2) * p * L_m * (I_{sq} * I_{rd} - I_{sd} * I_{rq})$.
5. **Convertors for back-to-back use:**
   - Utilize two six-switch-based converters, BTB, for vector control on the generator and GSC.
   - Implement the GOCA and IRFNN controller for AC–DC–AC power conversion.
   - Use vector control to optimize the generator's operation according to the DFIG's dynamical model in the d–q frame.
   - Employ the IRFNN for maintaining constant voltage independently of rotor magnitude and rotation direction.
   - Control reactive power using vector control.

6. **Active and reactive power exchange:**
   - Define the variables:
     - U_d, U_q: Grid voltage in the d–q axis (V),
     - I_{dg}, I_{qg}: Grid currents in the d–q axis (A).
   - Calculate active power (P_g) and reactive power (Q_g) using Eqs. (13) and (14):
     $P_g = (3/2) * (U_{dg} * I_{dg} - U_{qg} * I_{qg}) Q_g = (3/2) * (U_{qg} * I_{dg} - U_{dg} * I_{qg})$.
7. **Relationship between DC-link storage and grid power flow:**
   - Use Eq. (17) to relate electrical power generated or controlled by the power controller to the DC-link voltage and current.
8. **Ant colony optimization (ACO):**
   - Implement the ACO algorithm for optimization problems.
   - Utilize pheromone-based exchange of information for solving combinatorial optimization problems.
9. **IRFNN controller:**
   - Implement the IRFNN controller with memory terms and feedback loops.
   - Utilize Eqs. (18) to (22) for controlling nonlinear issues and improving convergence accuracy.

4. Result and discussion

This section of the research details the implementation carried out using the suggested technique, and the implementation tools are provided below.

4.1. Tool used

In this research, the authors used the Matrix Laboratory (MATLAB) tool to obtain the results. MATLAB was created by MathWorks and is a commercial programming language and numerical computing environment that supports many examples. Matrix processes, charting of functions and information, procedure development, user interface design, and linking with other programming languages are all probable with MATLAB. The findings provided to support the suggested effort stated below are as follows.

4.2. Result 1

Figure 4(a) illustrates that as a result, when the pitch angle increases the real power rises with the tidal step and is subsequently held constant at the rated power Pn. As can be seen in Fig. 4(b), the reactive power is maintained in an oscillating range close to zero independent of the input tidal speed. Reducing the cost per kilowatt-hour of energy production involves increasing the turbine's capacity factor. This can be achieved by specifying a rated flow speed for peak power generation and shedding power at speeds lower than the rated value.

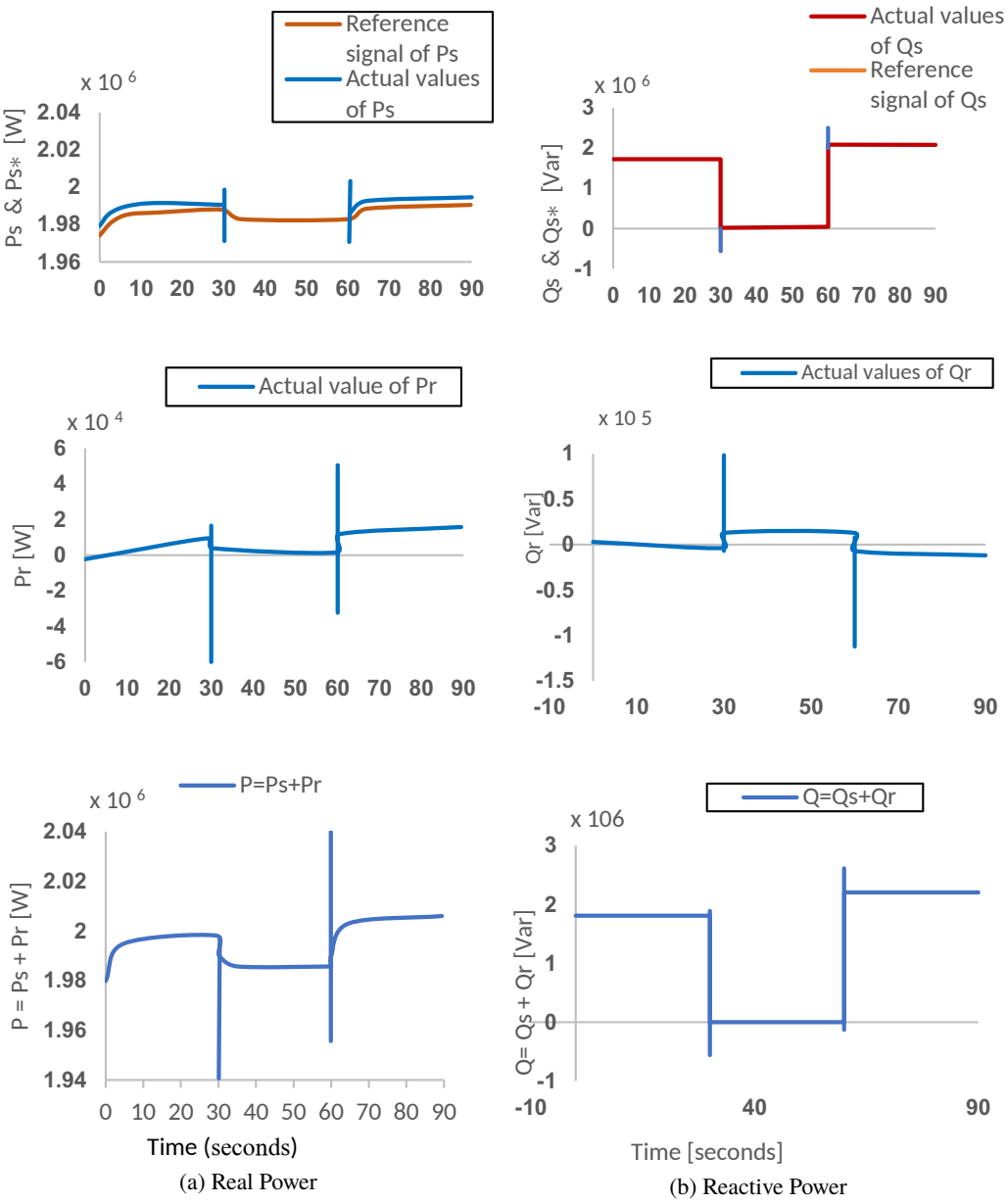

(a) Real Power (b) Reactive Power

Fig. 4. (a) Real Power (b) Reactive Power

4.3. Result 2

Figure 5 shows that the power coefficient is kept at an optimum value by the switching controller (C_p = 1.8 to 1.9), and thereafter it drops, indicating that the controller is performing properly.

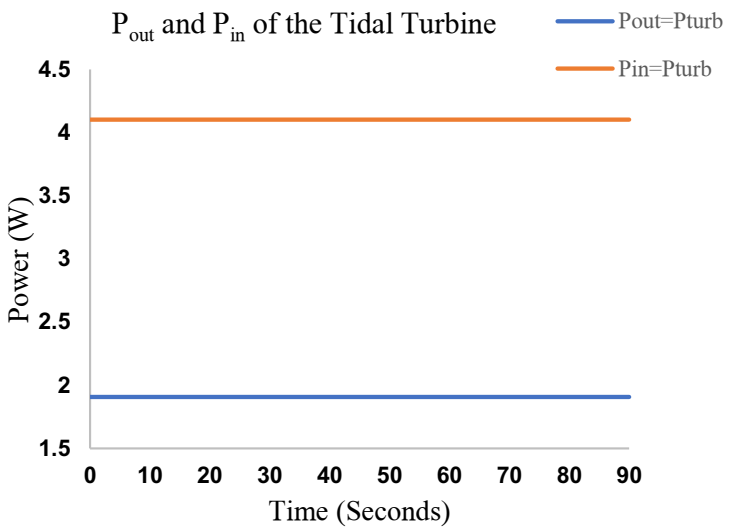

Fig. 5. P_{out} and P_{in} of the tidal turbine

As shown in Fig. 6, however, while operating in power restriction mode, the pitch angle is maintained at zero while the rotation speed varies, eventually reaching a value of the angular position of around (β ref = 2.67° to 2.77°).

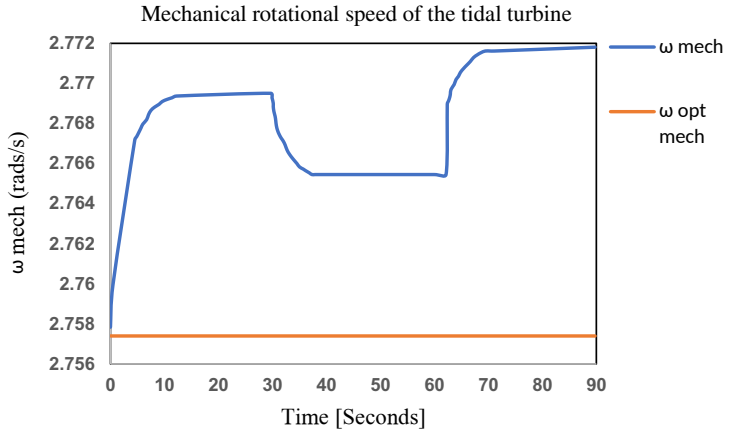

Fig. 6. Mechanical rotational speed of the tidal turbine

4.4. Result 3

The aerodynamic forces exerted on a turn could be easily adjusted by manipulating the pitch angle. The tidal turbine's actual power, P_t, and the maximum power, $P_{\max}$, are sent into the pitch controller. $P_{\max}$ is equivalent to 1.5 megawatt, the maximum power that could be produced by the generator. The difference between P_t and $P_{\max}$ is used by the PI to determine the pitch angle. The pitch angle has a range of 0 degrees to 21 degrees, as illustrated in Fig. 7. Moreover, there is

a restriction placed on the degree to which the pitch angle changes over time. The pitch angle rate of WTs could be anything from 3°/s to 10°/s. The rate of pitch angle employed in this research is about 10 degrees per second for big turbine sizes.

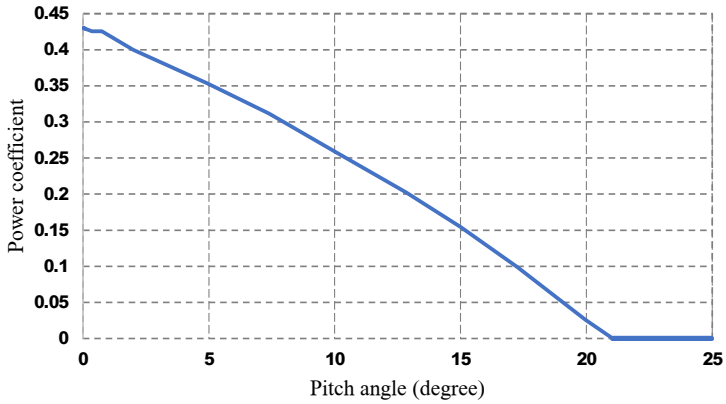

Fig. 7. Power coefficient versus pitch angle

4.5. Result 4

Figure 8 depicts the monthly fluctuations in the semidiurnal tide that could be seen in Raz de Sein, Brittany, France. The period of these tides, which includes both the spring and neap tides, is around 10 hours and 25 minutes. A tidal current's kinetic energy flow is proportional to the velocity of water moving over the channel's cross-section. It is denoted by the symbol (W/m^2), as defined by:

$$P = \frac{1}{2}\rho \int_A \frac{V^3 \mathrm{d}A}{A}. \tag{23}$$

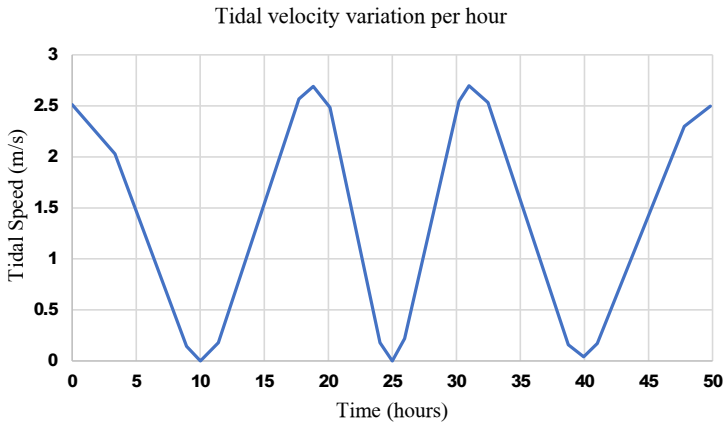

Fig. 8. Tidal velocity

This equation calculates fluid density (ρ) by dividing the area (A) of the turbine rotor by the component (V) of current flow velocity perpendicular to the channel cross-section, expressed in kilograms per cubic meter (kg/m^3).

5. Conclusion and future scope

The tidal turbines' smaller rotor mass means that could only supply a fraction of the frequency stability of generating units, even though tidal power is increasingly being integrated into the power grid. Hence, this results in a low-inertia power supply, which in turn leads to frequency issues. The identical parts used in WTs are also used in TSTs, which transforms tidal power into electricity. As a result of this, TSTs seem incredibly common to WTs even though they are covered undersea. This research focuses on a novel DFIG control scheme utilizing IRFNN and GACO techniques for improved operation. The observed findings indicate that the suggested controls give an enhancement in output power efficiency in a variety of operating modes. In the future, the rotor speed and power of the DFIG will achieve the measured value by using the described controllers. Hence, the suitable control legislation allows the tidal turbine to run reliably.

References

[1] Benbouzid M.E.H., Titah-Benbouzid H., Zhou Z., *Ocean Energy Technologies*, In: Abraham M.A. (Ed.), Encyclopedia of Sustainable Technologies, Elsevier, ISBN: 978-0-128-04677-7, pp. 73–85 (2017), DOI: 10.1016/B978-0-12-409548-9.10097-1.

[2] Benbouzid Mohamed, Yassine Amirat, Elhoussin Elbouchikhi, Marine Tidal and Wave Energy Converters: Technologies, Conversions, Grid Interface, Fault Detection, and Fault-Tolerant Control, MDPI (2020).

[3] Zainol Mohd Zaifulrizal, Nuraihan Ismail, Ismail Zainol, Abu A., Dahalan W., *A review on the status of tidal energy technology worldwide*, Sci. Int., vol. 29, no. 3, pp. 659–667 (2017).

[4] Toumi Sana, Elhoussin Elbouchikhi, Mohamed Benbouzid, Yassine Amirat, *Grid fault-resilient control of a PMSG-based tidal stream turbine*, Journal of Electrical Systems, vol. 16, no. 4, pp. 429–447 (2020).

[5] Che Hang Seng, Emil Levi, Martin Jones, Wooi-Ping Hew, Nasrudin Abd Rahim, *Current control methods for an asymmetrical six-phase induction motor drive*, IEEE Transactions on Power Electronics, vol. 29, no. 1, pp. 407–417 (2013), DOI: 10.1109/TPEL.2013.2248170.

[6] Zhu Donghai, Xudong Zou, Lu Deng, Qingjun Huang, Shiying Zhou, Yong Kang, *Inductance-emulating control for DFIG-based wind turbine to ride-through grid faults*, IEEE Transactions on power electronics, vol. 32, no. 11, pp. 8514–8525 (2016), DOI: 10.1109/TPEL.2016.2645791.

[7] Piyasinghe Lakshan, Zhixin Miao, Javad Khazaei, Lingling Fan, *Impedance model-based SSR analysis for TCSC compensated type-3 wind energy delivery systems*, IEEE Transactions on Sustainable Energy, vol. 6, no. 1, pp. 179–187 (2014), DOI: 10.1109/TSTE.2014.2362499.

[8] Cardenas Roberto, Rubén Peña, Salvador Alepuz, Greg Asher, *Overview of control systems for the operation of DFIGs in wind energy applications*, IEEE Transactions on Industrial Electronics, vol. 60, no. 7, pp. 2776–2798 (2013), DOI: 10.1109/TIE.2013.2243372.

[9] Nian Heng, Yipeng Song, *Direct power control of doubly fed induction generator under distorted grid voltage*, IEEE Transactions on Power Electronics, vol. 29, no. 2, pp. 894–905 (2013), DOI: 10.1109/TPEL.2013.2258943.

[10] Li Longqi, Heng Nian, Lijie Ding, Bo Zhou, *Direct power control of DFIG system without phase-locked loop under unbalanced and harmonically distorted voltage*, IEEE Transactions on energy conversion, vol. 33, no. 1, pp. 395–405 (2017), DOI: 10.1109/TEC.2017.2741473.

[11] El Daoudi, Soukaina, Loubna Lazrak, Mustapha Ait Lafkih, *Sliding mode approach applied to sensorless direct torque control of cage asynchronous motor via multi-level inverter*, Protection and Control of Modern Power Systems, vol. 5, pp. 1–10 (2020), DOI: 10.1186/s41601-020-00159-7.

[12] Sun Dan, Xiaohe Wang, *Low-complexity model predictive direct power control for DFIG under both balanced and unbalanced grid conditions*, IEEE Transactions on Industrial Electronics, vol. 63, no. 8, pp. 5186–5196 (2016), DOI: 10.1109/TIE.2016.2570201.

[13] Cheng Chenwen, Peng Cheng, Heng Nian, Dan Sun, *Model predictive stator current control of doubly fed induction generator during network unbalance*, IET Power Electronics, vol. 11, no. 1, pp. 120–128 (2018), DOI: 10.1049/iet-pel.2017.0049.

[14] Xiong Pinghua, Dan Sun, *Backstepping-based DPC strategy of a wind turbine-driven DFIG under normal and harmonic grid voltage*, IEEE Transactions on Power Electronics, vol. 31, no. 6, pp. 4216–4225 (2015), DOI: 10.1109/TPEL.2015.2477442.

[15] Boubzizi Saïd, Hafedh Abid, Mohamed Chaabane, *Comparative study of three types of controllers for DFIG in wind energy conversion system*, Protection and Control of Modern Power Systems, vol. 3, no. 1, pp. 1–12 (2018), DOI: 10.1186/s41601-018-0096-y.

[16] Chen Junjie, Yi Liu, Wei Xu, *Nonparametric predictive current control for standalone brushless doubly fed induction generators*, In 2020 International conference on electrical machines (ICEM), IEEE, vol. 1, pp. 2189–2195 (2020), DOI: 10.1109/ICEM49940.2020.9270712.

[17] Benbouhenni Habib, Zinelaabidine Boudjema, Abdelkader Belaidi, *Intelligent SVM technique of a multi-level inverter for a DFIG-based wind turbine system*, International Journal of Digital Signals and Smart Systems, vol. 3, no. 1–3, pp. 4-19 (2019), DOI: 10.1504/IJDSSS.2019.103372.

[18] Wang Yingzhao, Slobodan Đukanović, Nur Sarma, Siniša Djurović, *Implementation and performance evaluation of controller signal embedded sensorless speed estimation for wind turbine doubly fed induction generators*, International Journal of Electrical Power & Energy Systems, vol. 148, 108968 (2023), DOI: 10.1016/j.ijepes.2023.108968.

[19] Tavoosi Jafar, Ardashir Mohammadzadeh, Bahareh Pahlevanzadeh, Morad Bagherzadeh Kasmani, Shahab S. Band, Rabia Safdar, Amir H. Mosavi, *A machine learning approach for active/reactive power control of grid-connected doubly fed induction generators*, Ain Shams Engineering Journal, vol. 13, no. 2, 101564 (2022): DOI: 10.1016/j.asej.2021.08.007.

[20] Sahri Younes, Salah Tamalouzt, Sofia Lalouni Belaid, Seddik Bacha, Nasim Ullah, Ahmad Aziz Al Ahamdi, Ali Nasser Alzaed, *Advanced fuzzy 12 dtc control of doubly fed induction generator for optimal power extraction in wind turbine system under random wind conditions*, Sustainability, vol. 13, no. 21, 11593 (2021), DOI: 10.3390/su132111593.

[21] Alhato Mohammed Mazen, Soufiene Bouallègue, *Thermal exchange optimization-based control of a doubly fed induction generator in wind energy conversion systems*, Indones. J. Electr. Eng. Comput. Sci., vol. 20, no. 3, pp. 1252–1260 (2020), DOI: 10.11591/ijeecs.v20.i3.pp1252-1260.

[22] Moreira Adson Bezerra, Tárcio André Dos Santos Barros, Vanessa Siqueira De Castro Teixeira, Ramon Rodrigues De Souza, Marcelo Vinicius De Paula, Ernesto Ruppert Filho, *Control of powers for wind power generation and grid current harmonics filtering from doubly fed induction generator: Comparison of two strategies*, IEEE, Access 7, pp. 32703–32713 (2019), DOI: 10.1109/ACCESS.2019.2899456.

[23] Abdelmalek Samir, Ahmad Taher Azar, and Djalel Dib, *A novel actuator fault-tolerant control strategy of dfig-based wind turbines using takagi-sugeno multiple models*, International Journal of Control, Automation and Systems, vol. 16, pp. 1415–1424 (2018), DOI: 10.1007/s12555-017-0320-y.

[24] Venkatesh M., Jagannath Yadav B., *A Novel Approach to Optimal Design of PI Controller of Doubly Fed Induction Generator using Particle Swarm Optimization*, Journal of Electrical Engineering & Technology, vol. 8, no. 1, pp. 9–16 (2017).

[25] Boudjema Zinelaabidine, Rachid Taleb, Youcef Djeriri, Adil Yahdou, *A novel direct torque control using second order continuous sliding mode of a doubly fed induction generator for a wind energy conversion system*, Turkish Journal of Electrical Engineering and Computer Sciences, vol. 25, no. 2, pp. 965–975 (2017), DOI: 10.3906/elk-1510-89.

[26] Ghefiri Khaoula, Soufiene Bouallègue, Izaskun Garrido, Aitor J. Garrido, Joseph Haggège, *Complementary power control for doubly fed induction generator-based tidal stream turbine generation plants*, Energies, vol. 10, no. 7, 862 (2017), DOI: 10.3390/en10070862.

[27] Ebrahimkhani Sadegh, *Robust fractional order sliding mode control of doubly fed induction generator (DFIG)-based wind turbines*, ISA Transactions, vol. 63, pp. 343–354 (2016), DOI: 10.1016/j.isatra.2016.03.003.

[28] Alberdi Mikel, Modesto Amundarain, Aitor Garrido, Izaskun Garrido, *Neural control for voltage dips ride-through of oscillating water column-based wave energy converter equipped with doubly fed induction generator*, Renewable Energy, vol. 48, pp. 16–26 (2012), DOI: 10.1016/j.renene.2012.04.014.

[29] Dorigo Marco, Vittorio Maniezzo, Alberto Colorni, *Ant system: optimization by a colony of cooperating agents*, IEEE Transactions on Systems, Man, and Cybernetics, Part B (Cybernetics), vol. 26, no. 1, pp. 29–41 (1996), DOI: 10.1109/3477.484436.

[30] Jiang Song, Minjie Lian, Caiwu Lu, Qinghua Gu, Shunling Ruan, Xuecai Xie, *Ensemble prediction algorithm of anomaly monitoring based on big data analysis platform of open-pit mine slope*, Complexity 2018 (2018), DOI: 10.1155/2018/1048756.

[31] Luo Jie, Huiling Chen, Yueting Xu, Hui Huang, Xuehua Zhao, *An improved grasshopper optimization algorithm with application to financial stress prediction*, Applied Mathematical Modelling, vol. 64, pp. 654–668 (2018), DOI: 10.1016/j.apm.2018.07.044.

[32] Ren Zhengru, Roger Skjetne, Zhen Gao, *A crane overload protection controller for blade lifting operation based on model predictive control*, Energies, vol. 12, no. 1, 50 (2018), DOI: 10.3390/en12010050.

[33] Zhang Qian, Huiling Chen, Jie Luo, Yueting Xu, Chengwen Wu, Chengye Li, *Chaos enhanced bacterial foraging optimization for global optimization*, IEEE Access 6, pp. 64905–64919 (2018), DOI: 10.1109/ACCESS.2018.2876996.

[34] Guo Shikai, Rong Chen, Hui Li, Jian Gao, Yaqing Liu, *Crowdsourced Web application testing under real-time constraints*, International Journal of Software Engineering and Knowledge Engineering, vol. 28, no. 6, pp. 751–779 (2018), DOI: 10.1142/S0218194018500213.

[35] Ren Zhengru, Roger Skjetne, Zhiyu Jiang, Zhen Gao, Amrit Shankar Verma, *Integrated GNSS/IMU hub motion estimator for offshore wind turbine blade installation*, Mechanical Systems and Signal Processing, vol. 123, pp. 222–243 (2019), DOI: 10.1016/j.ymssp.2019.01.008.

[36] Guo Shikai, Rong Chen, Miaomiao Wei, Hui Li, Yaqing Liu, *Ensemble data reduction techniques and multi-RSMOTE via fuzzy integral for bug report classification*, IEEE Access 6, pp. 45934–45950 (2018), DOI: 10.1109/ACCESS.2018.2865780.

[37] Wu Daqing, Jiazhen Huo, Gefu Zhang, Weihua Zhang, *Minimization of logistics cost and carbon emissions based on quantum particle swarm optimization*, Sustainability, vol. 10, no. 10, 3791 (2018), DOI: 10.3390/su10103791.

[38] Zhou Yingrui, Taiyong Li, Jiayi Shi, Zijie Qian, *A CEEMDAN and XGBOOST-based approach to forecast crude oil prices*, Complexity 2019, pp. 1–15 (2019), DOI: 10.1155/2019/4392785.

[39] Datta A., Nandakumar S., *A survey on bio inspired meta heuristic-based clustering protocols for wireless sensor networks*, In IOP Conference Series: Materials Science and Engineering, IOP Publishing, vol. 263, no. 5, 052026 (2017), DOI: 10.1088/1757-899X/263/5/052026/meta.

[40] Zhou Junchao, Zixue Du, Yinghua Liao, Aihua Tang, *An optimization design of vehicle axle system based on multiobjective cooperative optimization algorithm*, Journal of the Chinese Institute of Engineers, vol. 41, no. 8, pp. 635–642 (2018), DOI: 10.1080/02533839.2018.1534559.

[41] Yang Ai-Min, Xiao-Lei Yang, Jin-Cai Chang, Bin Bai, Fan-Bei Kong, Qing-Bo Ran, *Research on a fusion scheme of cellular network and wireless sensor for cyber physical social systems*, IEEE Access 6, pp. 18786–18794 (2018), DOI: 10.1109/ACCESS.2018.2816565.

[42] Liu Yaqing, Xiaokai Yi, Rong Chen, Zhengguo Zhai, Jingxuan Gu, *Feature extraction based on information gain and sequential pattern for English question classification*, IET Software, vol. 12, no. 6, pp. 520–526 (2018), DOI: 10.1049/iet-sen.2018.0006.

[43] Huang Faming, Chi Yao, Weiping Liu, Yijing Li, Xiaowen Liu, *Landslide susceptibility assessment in the Nantian area of China: a comparison of frequency ratio model and support vector machine*, Geomatics, Natural Hazards and Risk, vol. 9, no. 1, pp. 919–938 (2018), DOI: 10.1080/19475705.2018.1482963.

[44] Guo Shikai, Yaqing Liu, Rong Chen, Xiao Sun, Xiangxin Wang, *Improved SMOTE algorithm to deal with imbalanced activity classes in smart homes*, Neural Processing Letters, vol. 50, pp. 1503–1526 (2019), DOI: 10.1007/s11063-018-9940-3.

[45] Sun Fengrui, Yuedong Yao, Xiangfang Li, *The heat and mass transfer characteristics of superheated steam coupled with non-condensing gases in horizontal wells with multi-point injection technique*, Energy, vol. 143, pp. 995–1005 (2018), DOI: 10.1016/j.energy.2017.11.028.

[46] Deng Wu, Junjie Xu, Huimin Zhao, *An improved ant colony optimization algorithm based on hybrid strategies for scheduling problem*, IEEE access, vol. 7, pp. 20281–20292 (2019), DOI: 10.1109/ACCESS.2019.2897580.

[47] Lu Kai-Hung, Hsin-Chuan Chen, Chiou-Jye Huang, Zhi-Feng Huang, *Design of IRFNN for reconfigured UPFC to power flow control and stability improvement*, In 2017 International Conference on Machine Learning and Cybernetics (ICMLC), IEEE, vol. 2, pp. 436–443 (2017), DOI: 10.1109/ICMLC.2017.8108959.